RSC Advances

PAPER

View Article Online
View Journal | View Issue

Cite this: *RSC Adv.*, 2023, **13**, 36181

Preparation of hydrophobic porous Au–Ag alloy nanoparticle arrays and their SERS properties†

Ming Kong,[a] Yingyi Wu,[b] Dandan Men,[b] Qianqian Ding[a] and Honghua Zhang*[b]

In this study, we prepared porous Au–Ag alloy nanoparticle arrays with hydrophobic surfaces through the polystyrene colloidal crystal template combined with the chemical etching method to realize rapid SERS detection for biochemical molecules. In the preparation process, the pore size of Au–Ag alloy nanoparticles could be adjusted by changing the deposition time of the Ag element. Furthermore, after depositing the Au film on the surface of the porous nanoparticle arrays, their surface changed from hydrophilic to hydrophobic. The hydrophobic surface can drive target molecules to locally aggregate. Meanwhile, the hydrophobic surface also possessed a large number of active "hot spots" due to the porous structure. For these reasons, the porous Au–Ag alloy nanoparticle arrays can enable rapid and trace SERS detection, which provide the material basis for the subsequent construction of the high-quality SERS substrate.

Received 15th September 2023
Accepted 26th November 2023

DOI: 10.1039/d3ra06284h

rsc.li/rsc-advances

1. Introduction

As a powerful biochemical substance detection method, surface-enhanced Raman spectroscopy (SERS) has the advantages of low cost, high sensitivity, simple operation, non-destructive testing, and "fingerprint" recognition, which is favored by researchers.[1–4] SERS detecting technique is an exciting nondestructive spectroscopic approach that could identify various biochemical organic molecules adsorbed on the nano-scaled noble metal surface, even single-molecule fingerprint-vibration signals. Compared with common spectral detection methods, it is not only more sensitive but also there is no interference from water molecules during testing.[5,6] In order to obtain the ideal performance of SERS techniques, it is essential to prepare uniform and sensitive SERS substrates. Therefore, researchers are committed to preparing high-quality SERS substrates.[7–10]

In order to obtain high-quality and high-sensitivity SERS substrates, various orderly metal nanostructure arrays with hydrophobic surfaces were used as SERS substrates.[11–14] For example, Zhang and co-workers prepared Cu–Ag bimetallic micro/nanostructure arrays on a Cu foil by using electrochemical deposition combined with lithography.[15] As a super-hydrophobic SERS substrate, the Cu–Ag bimetallic micro/nanostructure arrays realized the detection of 10^{-6} M crystal violet. Gentile's research group prepared micron-size Si column arrays by deep reactive ion etching (DRIE) technology and then deposited a layer of an Ag film on the top of the column by electroless plating method to obtain micron-size Si column@Ag nanoparticle arrays.[16] Due to their super-hydrophobic surfaces, the micron-size Si column@Ag nanoparticle arrays could detect rhodamine B with a concentration of 10^{-10} M. Yang's research group prepared a hydrophobic PS–Ag composite nanostructure array film by electrodepositing a layer of Ag film on the surface of the monolayer polystyrene (PS) colloidal sphere array, realizing the low concentration detection of rhodamine B, protein and virus.[17] However, although these methods can construct large-area and highly controllable super-hydrophobic micro/nanostructure arrays to realize highly sensitive SERS detection, these methods needed complex preparation processes and required expensive and precise equipment, so they were disadvantageous for practical applications.

In this study, porous Au–Ag alloy nanoparticle arrays were prepared by a simple route. First, the Au nanoparticle arrays were synthesized as previously reported.[18,19] Then, a layer of Ag film was deposited on the prepared Au nanoparticle arrays, followed by thermal annealing to form solid Au–Ag alloy nanoparticle arrays. After etching less-stable Ag from the solid Au–Ag alloy nanoparticles, porous Au–Ag alloy nanoparticle arrays were obtained. Importantly, after depositing the Au film on the surface of the porous nanoparticle arrays, their surface changed from hydrophilic to hydrophobic. The hydrophobic surface can drive target molecules to locally aggregate. Meanwhile, the hydrophobic surface also possessed a large number

[a]*Department of Precision Manufacturing Engineering, Suzhou Vocational Institute of Industrial Technology, Suzhou, 215104, China*

[b]*Jiangxi Key Laboratory of Material Surface Engineering, School of Material and Energy, Jiangxi Science and Technology Normal University, Nanchang 330013, China. E-mail: 15270008537@163.com*

† Electronic supplementary information (ESI) available. See DOI: https://doi.org/10.1039/d3ra06284h

of active "hot spots" due to the porous structure. For these reasons, the porous Au–Ag alloy nanoparticle arrays achieved rapid and trace SERS detection for biochemical molecules, which solved the problem of long-time immersion before the SERS test.

2. Materials and methods

2.1 Materials

PS colloidal ball suspension (2.5 wt%) was purchased from Alfa Aesar. Au and Ag targets used in sputtering deposition were purchased from Zhongnuo New Materials (Beijing) Technology Co., Ltd. All reagents were directly used without further purification. Deionized water with 18.2 MΩ cm was obtained using a Millipore Milli-Q gradient system.

2.2 Characterization

The surface morphology was observed by using scanning electron microscopy (SEM, Zeiss). The energy dispersive X-ray spectroscopy (EDS) and EDS elemental mappings of the samples were performed on a SmartEDX analysis system. The SERS signals were obtained on a portable Raman spectrometer (Accuman SR). X-ray photoelectron spectroscopy (XPS) data was obtained on a Thermo Scientific K-Alpha X-ray photoelectron spectrometer using Al as the excitation source. Contact angles were obtained using a HARKE-SPCA contact angles meter.

2.3 Preparation of Au nanoparticle arrays

In the experiment, the monolayer PS colloidal crystal arrays with periodic length of 500 nm were prepared by gas–liquid interface self-assembly.[20,21] Then, a layer of Au film was deposited on the surface of the PS colloidal crystal arrays using an ion-sputtering device (Cressington Sputter Coater 108). Finally, the Au nanoparticle arrays were obtained by annealing at different temperatures (200 °C, 400 °C, 600 °C, 800 °C, and 1000 °C) for 2.5 h.

2.4 Preparation of hydrophobic Au–Ag nanoparticle arrays

A layer of Ag film was deposited on the surface of the Au nanoparticle arrays, followed by annealing under N_2 and H_2 mixed gas (2 h) to obtain orderly arrays of Au–Ag alloy nanoparticles. Finally, the obtained orderly arrays of Au–Ag alloy nanoparticles were etched with 50% HNO_3, forming porous Au–Ag alloy nanoparticle arrays. In order to obtain a hydrophobic surface, a layer of Au film was deposited on the porous Au–Ag alloy nanoparticle arrays. The whole preparation process of the porous Au–Ag alloy nanoparticle arrays with the hydrophobic surface is shown in Fig. 1.

3. Results and discussion

3.1 Au nanoparticle arrays

PS colloidal crystals monolayer films was assembled on the quartz substrate, and a layer of Au film (deposition time: 60 s) was deposited on its surface using an ion-sputtering instrument, as shown in Fig. 2a. Then, it was annealed at different temperatures (200 °C, 400 °C, 600 °C, 800 °C, and 1000 °C) for 2.5 hours. The results showed that when the annealing temperature was 200 °C, the PS nanospheres did not melt and decompose completely, but the Au film on the surface melted (Fig. 2b). When the temperature increased to 400 °C, the PS nanospheres were completely melted and decomposed, and the deposited Au film was fused *in situ* to form Au nanoparticles with a hexagonal close-packed (hcp) arrangement. However, due to the low annealing temperature, some Au nanoparticles did not have enough energy to migrate, so there were some small Au nanoparticles in the array gap, as displayed in Fig. 2c. As the temperature was further increased to 600 °C and 800 °C, there were still some scattered small Au nanoparticles in the array gap, as shown in Fig. 2d and e. When the annealing temperature reached 1000 °C, there were no obvious small Au nanoparticles in the array gap, and the obtained Au nanoparticles were near-spherical with a regular and orderly arrangement, as shown in Fig. 2f. Therefore, 1000 °C was selected for the preparation of the Au nanoparticle arrays.

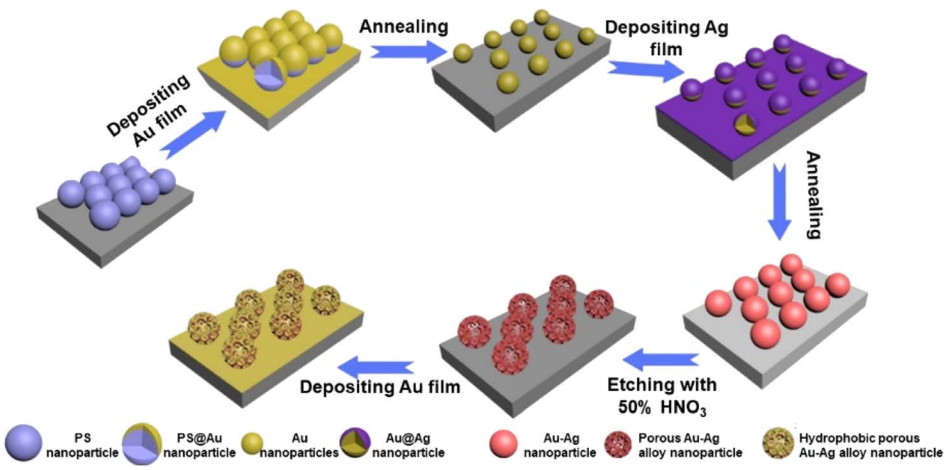

Fig. 1 Preparation process diagram of the porous Au–Ag alloy nanoparticle arrays with a hydrophobic surface.

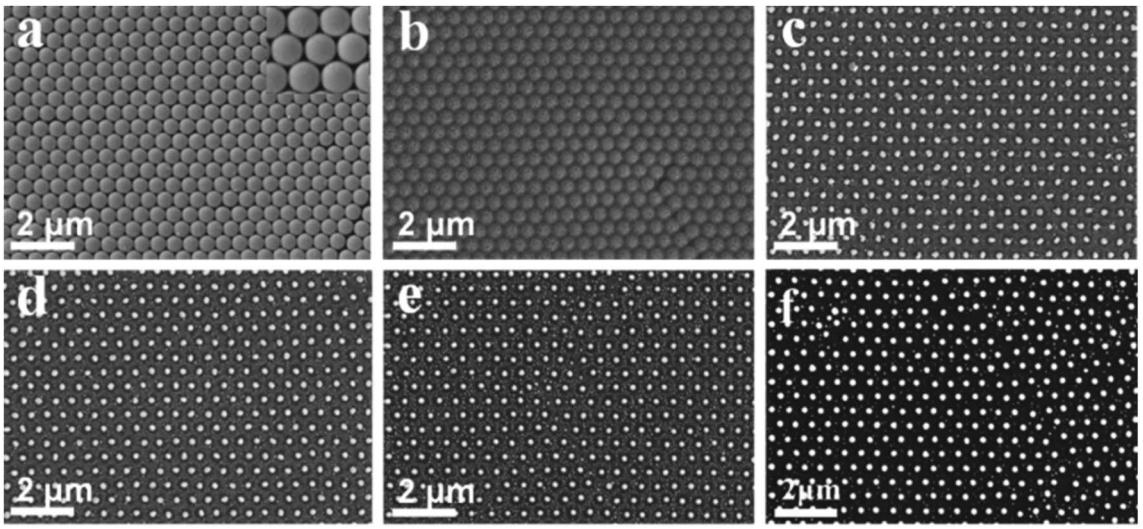

Fig. 2 SEM images of the Au nanoparticle arrays with a period length of 500 nm after annealing at different temperatures: (a) 0 °C, (b) 200 °C, (c) 400 °C, (d) 600 °C, (e) 800 °C, and (f) 1000 °C.

3.2 Au–Ag alloy nanoparticle orderly array

A layer of Ag film was deposited on the surface of the Au nanoparticle arrays, and solid Au–Ag alloy nanoparticle arrays were obtained by annealing. As displayed in Fig. 3, the size of Au–Ag nanoparticles gradually increased with the increase of the Ag film deposition time. When the deposition time of Ag film reached 180 s, agglomeration occurred, as shown in Fig. 3f. Therefore, when the deposition time of the Au film was 60 s, the deposition time of the Ag film should not exceed 150 s. EDS element mappings and EDS spectrum further confirmed that the obtained nanoparticle arrays were made up of Au and Ag elements, as shown in Fig. S1a–d.† Based on the above results, it can be concluded that the solid Au–Ag alloy nanoparticle arrays were successfully prepared.

3.3 Porous Au–Ag alloy nanoparticle orderly arrays

Taking advantage of the different activities of Ag and Au elements, porous Au–Ag alloy nanoparticle arrays with different nanopore sizes were obtained by etching the as-prepared Au–Ag alloy nanoparticle arrays in a 50% HNO_3 solution. As shown in Fig. 4a, when the deposition time of the Ag film was 60 s, there was no obvious porous structure after HNO_3 etching. When the deposition time of the Ag film increased to 90 s, the sample showed an obvious porous structure after etching, as displayed in Fig. 4b. With further increase of the deposition time of the Ag film, the pore size of Au–Ag nanoparticles gradually increased, as shown in Fig. 4c and d. The presence of a large number of nanopores can generate a large number of active "hot spots" to effectively enhance the SERS effect, especially for nanopores with

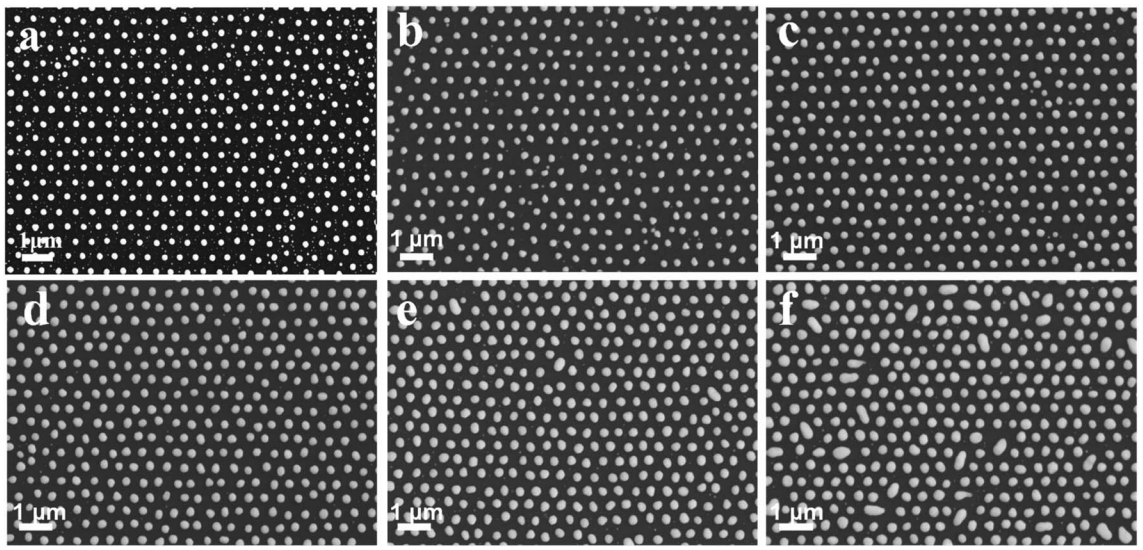

Fig. 3 SEM images of the Au–Ag alloy nanoparticle orderly arrays with different deposition times: (a) 0 s, (b) 60 s, (c) 90 s, (d) 120 s, (e) 150 s, and (f) 180 s.

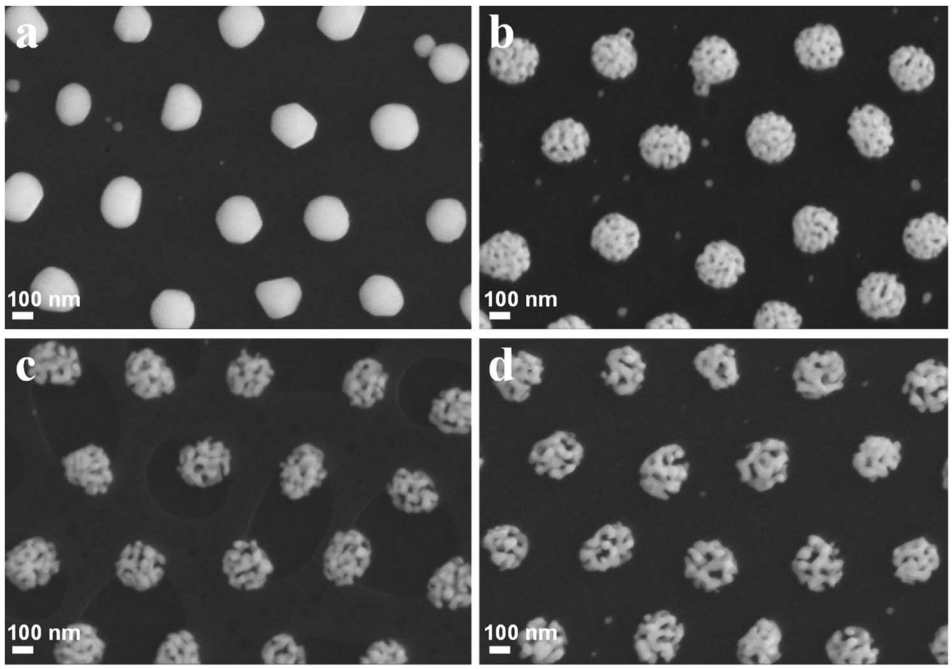

Fig. 4 SEM images of the porous nanoparticle orderly arrays obtained by different Ag deposition times: (a) 60 s, (b) 90 s, (c) 120 s, and (d) 150 s.

a size less than 10 nm.[22,23] Moreover, the presence of nanopores also increases the specific surface area of the particles, which is conducive to the adsorption of target molecules. However, when the deposition time of the Ag film reached 120 s and 150 s, it could be seen that most nanopore sizes exceeded 10 nm, as shown in Fig. 4c and d, which were unfavourable for the enhancement of the SERS signal. Furthermore, Fig. 5 shows the corresponding EDS elemental mapping and EDS spectrum of the porous nanoparticle arrays with the Ag film deposition time of 90 s. It revealed that the porous nanoparticle arrays were composed of Au and Ag elements. Among them, the Au element was the main element. To further verify the formation of the porous Au–Ag alloy nanoparticle arrays, the valence states of Au and Ag were investigated by XPS, as shown in Fig. 6. Fig. 6b presents the Au 4f spectrum energy region. The peaks at 83.4 and 87.1 eV were ascribed to the metallic Au $4f_{7/2}$ and Au $4f_{5/2}$,

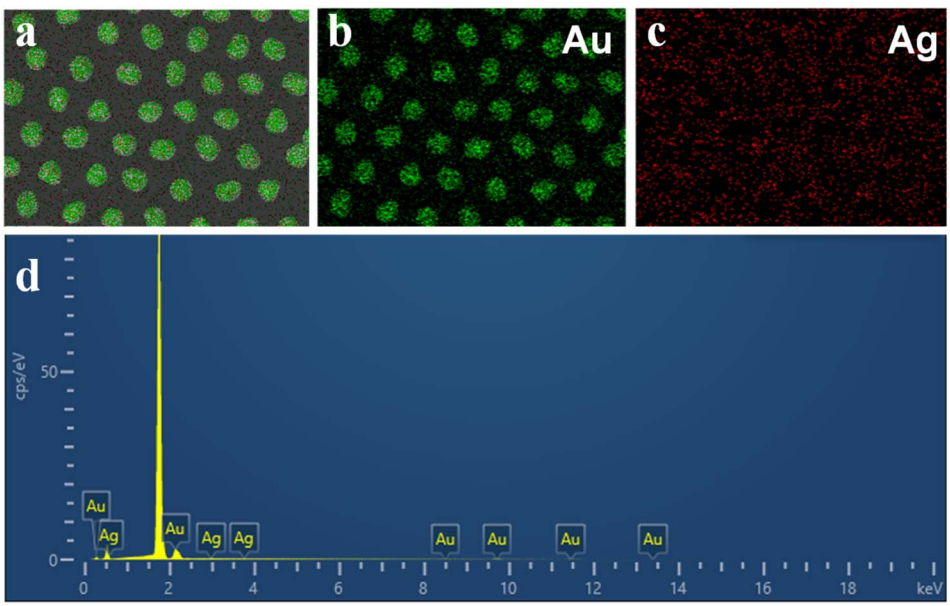

Fig. 5 (a–c) EDS elemental mapping images and EDS spectrum (d) of the porous nanoparticles orderly arrays obtained with Ag deposition time of 90 s.

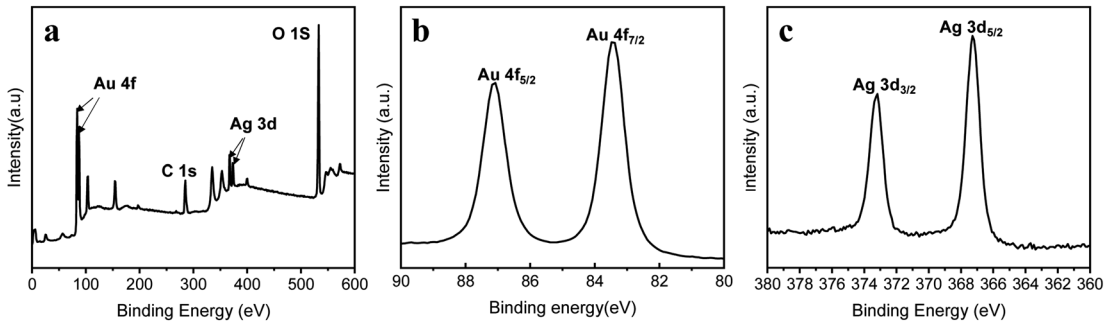

Fig. 6 XPS spectra of the porous nanoparticle arrays: (a) a survey scan, (b) Au 4f energy region, and (c) Ag 3d energy region.

respectively.[24] Fig. 6c presents the Ag 3c spectrum energy region. The peaks at 367.3 and 373.2 eV were ascribed to the metallic Ag $3d_{5/2}$ and Ag $3d_{3/2}$, respectively.[24,25] The XPS measurements showed that both Au and Ag in the porous nanoparticle arrays were zero-valent, further demonstrating that the prepared nanoparticle arrays were porous Au–Ag alloy nanoparticle arrays.

3.4 Wettability test

After depositing the Au film on the surface of the porous Au–Ag alloy nanoparticle arrays (b1–b4), their surfaces changed from hydrophilic to hydrophobic, as shown in Fig. 7 and Table 1. From SEM images (Fig. S2†), it can be seen that the surface of the porous Au–Ag alloy nanoparticle arrays after depositing the Au film maintained their porous structure. The change of hydrophilicity for the surface of the porous Au–Ag alloy nanoparticle arrays may be due to the generated nano hierarchical structure caused by depositing the Au film.

In Fig. 7, a1–a4 are the images of the contact angles of the porous Au–Ag alloy nanoparticle arrays before depositing the Au film; b1–b4 are the images of the contact angle of the porous Au–Ag alloy nanoparticle arrays after depositing the Au film. According to Table 1, the contact angles of the porous Au–Ag alloy particle arrays were all less than 90°, indicating that they were hydrophilic. After depositing a layer of Au film, the surface of the porous Au–Ag alloy nanoparticle arrays changed from hydrophilic to hydrophobic, as shown in Fig. 7b1–b4, which may be due to the produced nano hierarchical structure of the surface of the porous nanoparticle arrays after the deposition of the Au film. The generation of hydrophobic surface can drive target molecules to locally aggregate, which is helpful to realize the rapid SERS detection of the target molecules. Moreover, the contact angle of the porous structure with an Ag film deposition time of 90 s was 128.77° after the deposition of the Au film. With the increase in pore size, the contact angle increased to 135.03°. However, as the pore size further increased, the contact angle decreased to 131.59°. This may be because the large pore size reduced the surface roughness.[26] Based on the above results, the sample b2 was selected and used as a SERS substrate.

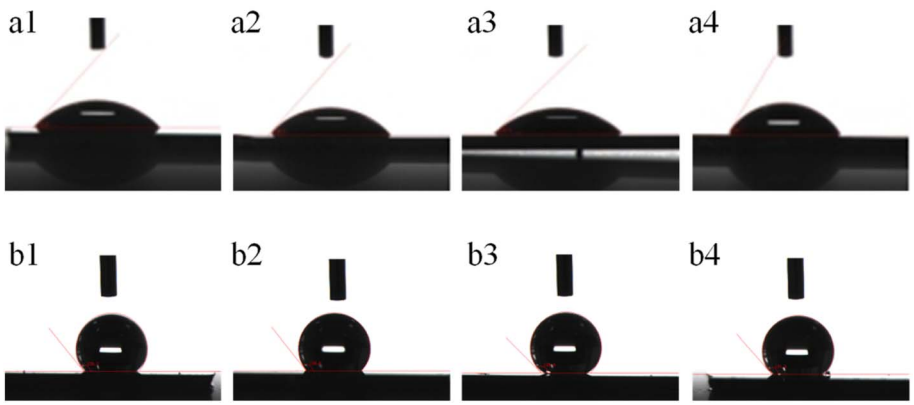

Fig. 7 Surface wettability contrast of the porous Au–Ag alloy nanoparticle arrays obtained with different Ag film deposition times (a1 and b1: 60 s, a2 and b2: 90 s, a3 and b3: 120 s, a4 and b4: 150 s): before (a1–a4) and after (b1–b4) Au film deposition.

Table 1 Contact angles of Au–Ag alloy nanoparticle arrays before and after depositing the Au film

Simple	Contact angle			
Before depositing	47.51° (a1)	48.06° (a2)	43.80° (a3)	58.71° (a4)
After depositing	129.18° (b1)	128.77° (b2)	135.03° (b3)	131.59° (b4)

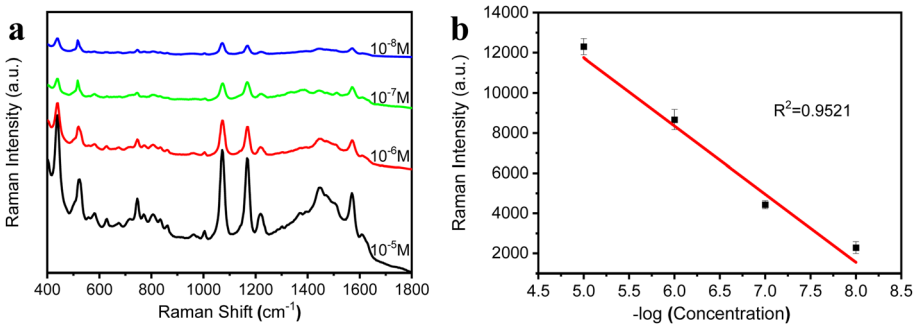

Fig. 8 (a) SERS spectra of 4-ATP with different concentrations using the porous Au–Ag alloy nanoparticle orderly arrays after depositing the Au film as the SERS substrate; (b) the linear calibration plot between the Raman intensity measured at the standard peaks (1073 cm^{-1}) and the concentrations of 4-ATP.

3.5 SERS performance

The hydrophobic surface has a rough microstructure and low surface energy, and this special structure is able to "lock in" air.[27,28] In this case, water droplets falling on its surface remain spherical, rather than spreading out. In this study, the porous Au–Ag alloy particle arrays with a hydrophobic surface (b2) was used as a SERS substrate for the detection of 4-ATP. Before SERS measurement, 20 μL 4-ATP solution with different concentrations (10^{-5} M, 10^{-6} M, 10^{-7} M, and 10^{-8} M) were dropped on the arrays. When the liquid evaporated completely, SERS spectra were measured. Fig. 8a shows the SERS spectra for 4-ATP with different concentrations. Fig. 8b presents a linear calibration plot between the Raman intensity measured at the standard peaks (1073 cm^{-1}) and the concentrations of 4-ATP. As shown in Fig. 8b, the detection limit of the porous Au–Ag alloy nanoparticles orderly arrays for 4-ATP was 4×10^{-9} M. These results showed that the porous Au–Ag alloy nanoparticles orderly arrays can realize the rapid, trace, and highly sensitive detection of 4-ATP molecules. This was mainly attributed to the presence of a large number of nanopores and hydrophobic surfaces of the porous Au–Ag alloy nanoparticle arrays. Therefore, the porous Au–Ag alloy nanoparticle arrays can solve the problem that the SERS substrates need to be soaked in the detection solution for a long time before testing, which is not conducive to practical applications.

4. Conclusions

In this study, porous Au–Ag alloy nanoparticle arrays with a hydrophobic surface as an SERS substrate were prepared by a simple method. In this method, the porous Au–Ag alloy nanoparticle arrays were obtained using the PS colloidal crystals template combined with depositing metal layer, annealing, and chemical etching. In the entire preparation process, expensive instrument was not required. At the same time, no surfactant was needed, which was conducive to the adsorption of target molecules on the surface of the SERS substrate. Additionally, the pore size of the porous Au–Ag alloy nanoparticles can be controlled by tuning the deposition time of the Ag element. After depositing the Au film on the surfaces of the porous nanoparticle arrays, their surface changed from hydrophilic to hydrophobic. The hydrophobic surface can drive target molecules to locally aggregate. Meanwhile, the hydrophobic surface also possessed a large number of active "hot spots" due to the porous structure. For these reasons, the porous Au–Ag alloy nanoparticle arrays achieved rapid and trace SERS detection. This method not only provides an implementation way for the preparation of high-quality SERS substrate but also can promote the practical application of 2D nanoparticle arrays for biochemical detection.

Conflicts of interest

There are no conflicts to declare.

Acknowledgements

The authors acknowledge financial support from the Natural Science Foundation of China (grant no. 52063015), supported by Jiangsu University Blue Project.

References

1 L. Yang, P. Li, H. Liu, X. Tang and J. Liu, *Chem. Soc. Rev.*, 2015, **44**, 2837–2848.
2 Z. Huang, G. Meng, X. Hu, Q. Pan, D. Huo, H. Zhou, Y. Ke and N. Wu, *Nano Res.*, 2019, **12**, 449–455.
3 B. Liu, G. Han, Z. Zhang, R. Liu and H. Wang, *Anal. Chem.*, 2012, **84**, 255–261.
4 M. Ge, P. Li, G. Zhou, S. Chen, W. Han, F. Qin, Y. Nie, Y. Wang, M. Qin, G. Huang, L. Yang and Z. Tian, *J. Am. Chem. Soc.*, 2021, **143**, 7769–7776.
5 Y. Zhou, J. Li, L. Zhang, Z. Ge, X. Wang, X. Hu, T. Xu, P. Li and W. Xu, *Anal. Bioanal. Chem.*, 2019, **411**, 5691–5701.
6 K. Zhang, Y. Liu, Y. Wang, J. Zhao and B. Liu, *Chem. Sci.*, 2019, **10**, 1741–1745.
7 H. Zhang, M. Liu, F. Zhou, D. Liu, G. Liu, G. Duan, W. Cai and Y. Li, *Small*, 2015, **18**, 844–853.
8 Q. Ding, L. Hang and L. Ma, *RSC Adv.*, 2018, **8**, 1753–1757.
9 K. Zhu, Z. Wang, S. Zong, Y. Liu, K. Yang, N. Li, Z. Wang, L. Li, H. Tang and Y. Cui, *ACS Appl. Mater. Interfaces*, 2020, **12**, 29917–29927.

10 X. Ha, S. An, H. Hao, L. Nan, C. Hang and W. Asi, *Anal. Sci.*, 2020, **36**, 667–674.
11 F. Chen, Y. Zhao, S. Zhang, S. Wei, A. Ming and C. Mao, *Biosensors*, 2022, **12**, 273–280.
12 M. Sakir, E. Yilmaz and M. Onses, *Microchem. J.*, 2020, **154**, 104628–104635.
13 K. Sivashanmugan, V. Nguyen and B. Nguyen, *Mater. Lett.*, 2020, **271**, 127807–127815.
14 C. Sun, S. Zhang, J. Wang and F. Ge, *Surf. Interfaces*, 2022, **28**, 101616–101621.
15 Q. Zhang, Y. Chen, Z. Guo, H. Liu, D. Wang and X. Huang, *ACS Appl. Mater. Interfaces*, 2013, **5**, 10633–10642.
16 F. Gentile, R. Rocca, G. Marinaro, A. Nicastri, A. Toma, F. Paonessa, G. Cojoc, C. Liberale, F. Benfenati and E. Fabrizio, *ACS Appl. Mater. Interfaces*, 2012, **4**, 2903–2911.
17 S. Yang, P. Hricko, P. Huang, S. Li, Y. Zhao, Y. Xie, F. Guo, L. Wang and T. Huang, *J. Mater. Chem. C*, 2014, **2**, 542–547.
18 L. Hang, F. Zhou, D. Men, H. Li, X. Li, H. Zhang, G. Liu, W. Cai, C. Li and Y. Li, *Nano Res.*, 2017, **10**, 2257–2270.
19 C. Xing, S. Zhong, J. Yu, X. Li, A. Cao, D. Men, B. Wu, W. Cai and Y. Li, *J. Mater. Chem. C*, 2020, **8**, 3838–3845.
20 X. Li, T. Zhang, J. Yu, C. Xing, X. Li, W. Cai and Y. Li, *ACS Appl. Mater. Interfaces*, 2020, **9**, 40702–40710.
21 Y. Sun, F. Hang, D. Men, H. Li and X. Li, *J. Mater. Chem. C*, 2016, **4**, 9864–9871.
22 C. Yonzon, C. Haynes, X. Zhang, J. Walsh and R. Van Duyne, *Anal. Chem.*, 2004, **76**, 78–85.
23 A. Haes, W. Hall, L. Chang, W. Klein and R. Duyne, *Nano Lett.*, 2004, **4**, 1029–1034.
24 T. Zhang, F. Zhou, L. Hang, Y. Sun, D. Liu, H. Li, G. Liu, X. Lyu, C. Li, W. Cai and L. Yue, *J. Mater. Chem. C*, 2017, **5**, 11039–11045.
25 X. Li, T. Zhang, J. Yu, C. Xing, X. Li, W. Cai and Y. Li, *ACS Appl. Mater. Interfaces*, 2020, **12**, 40702–40710.
26 H. Zhang, M. Liu, F. Zhou, D. Liu, G. Liu, G. Duan, W. Cai and Y. Li, *Small*, 2015, **11**, 844–853.
27 L. Wen, Y. Tian and L. Jiang, *Angew. Chem., Int. Ed.*, 2015, **54**, 3387–3399.
28 S. Pan, R. Guo and W. Xu, *Soft Matter*, 2014, **10**, 9187–9192.